symmetry

IMPACT FACTOR 2.940

CITESCORE 4.3

Review

Dilepton Program with Time-of-Flight Detector at the STAR Experiment

Xin Dong, Lijuan Ruan, Ming Shao, Yongjie Sun, Zebo Tang, Zhangbu Xu, Wangmei Zha and Yifei Zhang

Special Issue

Heavy-Ion Collisions and Multiparticle Production

Edited by

Prof. Dr. Qun Wang, Prof. Dr. Zuotang Liang and Prof. Dr. Enke Wang

MDPI

https://doi.org/10.3390/sym15020392

symmetry

MDPI

Review

Dilepton Program with Time-of-Flight Detector at the STAR Experiment

Xin Dong [1], Lijuan Ruan [2], Ming Shao [3], Yongjie Sun [3], Zebo Tang [3,*], Zhangbu Xu [2] and Wangmei Zha [3] and Yifei Zhang [3]

[1] Nuclear Science Division, Lawrence Berkeley National Laboratory, Berkeley, CA 94720, USA
[2] Physics Department, Brookhaven National Laboratory, Upton, NY 11973, USA
[3] State Key Laboratory of Particle Detection and Electronics, University of Science and Technology of China, Hefei 230026, China
* Correspondence: zbtang@ustc.edu.cn

Abstract: Pairs of lepton and antilepton (dilepton) in a continuous mass range are one of the most experimentally challenging and golden probes of the quark-gluon plasma (QGP) produced in heavy ion collisions because they do not strongly interact with the hot and dense medium, and reflect the properties of the medium at the time the dilepton is generated. The measurements of dileptons require lepton identification with high purity and high efficiency at large detector acceptance. STAR is one of two large experiments at the relativistic heavy ion collider with a primary goal of searching for the QGP and studying its properties. The STAR experiment launched a comprehensive dielectron (e^+e^-) program enabled by the time-of-flight (TOF) detector that had been fully installed in 2010. In this article, we review the decade-long *R*&*D*, the construction and performance of the STAR TOF detector, and dielectron measurements, including thermal dielectron production and dielectron production from the Breit–Wheeler process. Future perspectives are also discussed.

Keywords: quark gluon plasma; heavy ion collision; dilepton; chiral symmetry restoration; thermal radiation; strong magnetic field; Breit–Wheeler process

Citation: Dong, X.; Ruan, L.; Shao, M.; Sun, Y.; Tang, Z.; Xu, Z.; Zha, W.; Zhang, Y. Dilepton Program with Time-of-Flight Detector at the STAR Experiment. *Symmetry* **2023**, *15*, 392. https://doi.org/10.3390/sym15020392

Academic Editor: Sergei D. Odintsov

Received: 28 December 2022
Revised: 14 January 2023
Accepted: 30 January 2023
Published: 2 February 2023

1. Introduction

Quark–gluon plasma (QGP) consists of fundamental building blocks of matter at the most extreme temperature and density conditions. QGP existed briefly during the first few microseconds after the Big Bang and can be recreated in ultrarelativistic heavy-ion collisions in which quarks and gluons are liberated from confinement within nucleons. The thermodynamic and hydrodynamic properties of the QGP, such as temperature and viscosity, have been under intense investigation by means of theoretical lattice quantum chromodynamic (QCD) computations [1,2], and in experiments utilizing the world's most powerful supercomputers and particle accelerators [3,4]. Thermal lepton pairs (e^+e^- and $\mu^+\mu^-$) from QGP radiation [5–7] are penetrating probes of the true temperature of the emitting source and are considered the holy grail of the study of QGP since they do not suffer from either final state interactions or the blue-shift effects from collective motion [8–11].

Despite the focus on nuclear physics, heavy-ion collisions have been understood as an opportunistic tool for studying quantum electrodynamics (QED) in unique regimes for nearly a century [12,13], and have attracted significant interest in the last 40 years [14–16], with generations of powerful accelerators. Some of the earliest measurements of electromagnetic processes in heavy-ion collisions were studied by the BEVALAC at LBNL [17], the AGS at BNL [18], and by the SPS at CERN [19]. In 2000, the relativistic heavy ion collider (RHIC) began operation and ushered in a new era of high-energy nuclear physics with ultrarelativistic Au beams, providing collisions with a center-of-mass energy per nucleon pair from $\sqrt{s_{\rm NN}}$ = 200 GeV at top energy to 3.0 GeV in fixed-target mode. The payoff

from this next-generation facility was almost immediate, with all four RHIC experiments reporting the observation of a new state of nuclear matter in 2004: the QGP [20–23]. In an influential workshop in 1990 titled "Can RHIC be used to test QED?" [24], the top priority was said to be "to understand the validity of the best available descriptions of e^+e^- pair production in peripheral heavy-ion collisions, especially for the domain where this process is known to be nonperturbative (multiple pair production)". It positively concluded that "A study of electromagnetic phenomena in extremely peripheral collisions of relativistic heavy ions can become a rich and exciting field that will complement studies of central collisions." However, none of the three (Landau–Lifschtz, Bethe–Heitler and Breit–Wheeler) processes was explicitly mentioned. Right from the start of RHIC operation, the two "large" experiments at RHIC (STAR and PHENIX) studied the electromagnetic production of e^+e^- from the electromagnetic fields of colliding ultrarelativistic Au nuclei [25,26]. Multiple experiments performed measurements of the total cross-section of electromagnetically produced l^+l^- from ultraperipheral heavy-ion collisions [26–28] or from exclusive $p+p$ [29] collisions. Significant progress through multiple discoveries was achieved in the physics of photon interactions. Experimental measurements and theoretical descriptions have been progressing from the initial discoveries toward quantitative and precise comparisons. Polarized photons were used and proposed as a tool to test and define the photon Wigner function [30–36], to probe the properties of the QGP [37–43], to measure nuclear charge and mass radii [37,44–46], to study gluon structure inside nuclei [47–49], and to investigate new quantum effects [45,48,50–53]. The subject has evolved significantly in the last decade, with new measurements and a new understanding of thermal radiation and strong QED fields.

With the installation of a time-of-flight detector (TOF) surrounding the STAR time projection chamber (TPC) starting in 2009–2010, the combination demonstrated effective electron particle identification with the necessary purity and large acceptance in a very cost-effective configuration. We dedicate this review article to the relevant STAR TOF detector at the RHIC facility, with special attention given to its unique capabilities and limitations with respect to measuring thermal dielectron radiation from QGP and the novel QED phenomena, especially the Breit–Wheeler process and vacuum birefringence.

2. Time-of-Flight Detector

The multigap resistive plate chamber (MRPC) was first developed by the ALICE TOF group in the 1990s [54] to efficiently identify copiously produced charged particles in relativistic heavy ion collisions. As a new type of gaseous detector with precision timing performance, the MRPC is suitable for applications requiring a large area, high granularity, and low cost.

The MRPC in China was first developed by the high-energy physics group led by Prof. Hongfang Chen at the University of Science and Technology of China (USTC) in 2000, when the STAR experiment at RHIC sought to build an MRPC-based TOF to improve the identification capability of charged particles. USTC was responsible for the *R*&*D* of MRPC to meet the requirements of STAR TOF.

The first MRPC prototype was very simple, with only one readout pad and a sensitive area of about 3×3 cm^2 and five 0.22 mm thick gas gaps (see the left panel of Figure 1), aiming to verify the feasibility of this technique. In late 2000, the performance of this prototype was studied in the T10 test beam facility at CERN. The prototype functioned well, with a time resolution of 70 ps and detection efficiency of >95% (right panel of Figure 1) [55,56]. Soon after this success, a batch of MRPC modules with different structures were developed and tested [57]. Figure 2 shows the structure of an MRPC prototype with a sensitive area of 20×6.3 cm^2 and six gas gaps. The sensitive area was divided into 12 regions by 12 readout pads with a size of 3.1×3.0 cm^2. The time resolution of this prototype reached 60 ps, and its detection efficiency exceeded 97% in the beam test with good uniformity [57]. An MRPC prototype with the same sensitive area, but with two stacks of five gas gaps, was also constructed and tested. Its time resolution reached 50 ps, and its detection efficiency exceeded 99%. Considering the limited available space for STAR

TOF installation, the 6-gap MRPC structure was chosen for the STAR TOF. The readout pads were recombined into a size of 3.1 × 6.1 cm^2 to reduce the total number of readout channels [58].

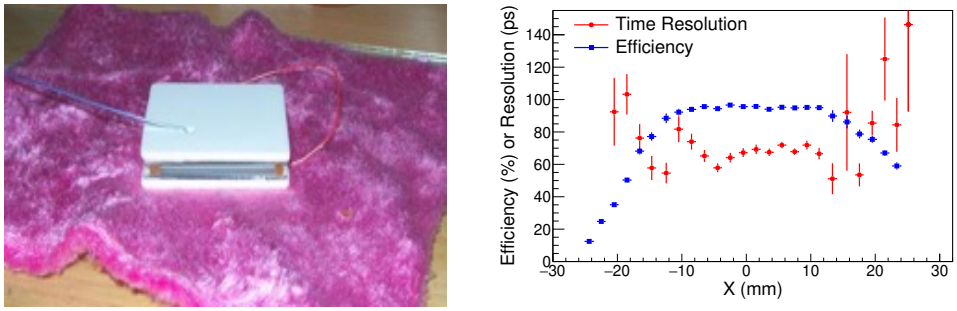

Figure 1. (**left**) The first MRPC module produced at USTC. (**right**) Detection efficiency and time resolution as a function of distance from the center of the readout pad [55].

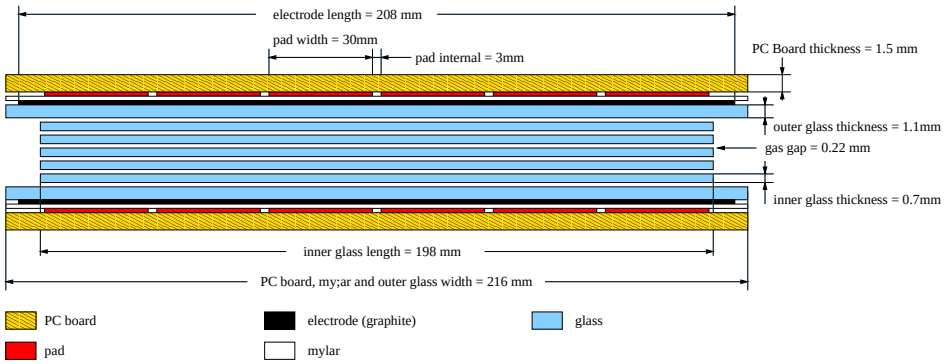

Figure 2. The structure of the MRPC prototype for STAR TOF.

In 2002, a TOF tray prototype (TOFr) with 28 MRPC modules was built by USTC and Rice university. A team led by Prof. Hongfang Chen tested the performance of the TOFr under various operating conditions at the AGS facility for 10 weeks prior to installation in the STAR experiment for the 2002–2003 physics run. The optimal parameters of high voltage, gas mixture, and threshold voltage for the operation of the prototype at STAR were determined from the beam test results [59]. TOFr was installed in STAR after the test at the AGS replacing one central trigger barrel module, and was part of the p+p and d+Au physics runs. In the STAR environment, the detection efficiency of the TOFr tray, averaged over all the channels, was around 95%, and the time resolution was 85 ps. The performance of the TOFr tray met the STAR physics goals and could significantly extend STAR particle identification capabilities [60]. With 2σ separation, protons/(pions + kaons) and kaons/pions were identified up to 3 and 1.6 GeV/c, respectively. Although the acceptance of the prototype was only 1/120 of the TOF system, several important physics results were achieved from the acquired data thanks to the extended particle identification capability [61,62]. With the success of the TOFr physics run, the STAR collaboration decided that all TOF MRPC modules were to be produced in China.

Thanks to the experiences of producing and operating the TOFr, and the extensive study of the MRPC technology [63–66], the production-process and quality-control requirements for MRPC module mass production for the STAR TOF were established. In 2006, funded by the National Natural Science Foundation of China, the Chinese Academy of Sciences, and the Ministry of Science and Technology, the Chinese STAR group launched the construction of the STAR TOF. By 2009, over 4000 MRPC modules were produced by Tsinghua University and USTC. Due to the strict quality management, the final yield was >95%, with excellent uniformity in performance [67,68]. The whole STAR barrel TOF consisted of 120 trays (each tray was analogous to the TOFr), 3840 MRPC modules, and 23,040 channels in total. It covered approximately the pseudo-rapidity interval (−1, 1) and

full azimuthal range. Operating with a 94.7% $C_2H_2F_4$ + 5.3% iso-Butane gas mixture, the MRPCs of the STAR barrel TOF showed a better intrinsic time resolution than 70 ps (the overall time resolution of STAR TOF also depended on the time jitter of the "start" time detector, which varied with different heavy ion collision systems). This time resolution and the corresponding particle identification capability were consistent with those achieved by TOFr and remained stable for more than 10 years of STAR operation.

After the success of the STAR TOF project, the USTC group continued to develop the MRPC technique and applied it to large facilities, such as a muon telescope detector and end-cap TOF for the STAR experiment, an end-cap TOF upgrade for the Beijing Spectrometer (BESIII), the TOF for the compressed baryonic matter (CBM) experiment, and the TOF for the CSR external-target experiment (CEE) [69].

3. Thermal Dileptons

Photons and dileptons (e^+e^- or $\mu^+\mu^-$) are emitted at various stages during the space-time evolution of the nuclear medium created in ultrarelativistic heavy-ion collisions. As penetrating electromagnetic probe dileptons do not suffer from strong interactions, they keep undistorted information of the sources from which the dileptons are coming. These sources are expected to contribute differently in lepton-pair invariant mass (M_{ll}), which are usually categorized into three regions:

(1) In the low-mass region (LMR), below ϕ mass ($M_{ll} < 1.1$ GeV/c^2), the main contributions are from light meson (π^0, η, ρ^0, ω, ϕ) decays or Dalitz decays. In particular, one can investigate hadronic in-medium properties via ρ^0 spectral modifications, which is sensitive to the mechanisms of chiral symmetry restoration in QCD matter [70]. Modified dilepton yields in LMR are expected to be related with the medium's lifetime and the transition from hadronic into partonic degrees of freedom [71].

(2) In the intermediate-mass region (IMR), namely, between ϕ and J/ψ mass ($M_{ll} \simeq 1.2$–3 GeV/c^2), the invariant-mass spectrum is continuum-like in both heavy flavor decays and nuclear matter emissions. This provides the chance to measure the direct radiation signals of QGP, which are expected to be a clean thermometer of the nuclear medium [10] by extracting the inverse slope of the mass spectra, which is unaffected by the blue shift of the expanding system.

(3) In the high-mass region (HMR), $M_{ll} \geq 3$ GeV/c^2, the main sources are heavy flavor/quarkonium decays and the Drell–Yan process.

Thermal dileptons from QGP radiation are of particular interest since they are sensitive to the properties of the produced medium. By investigating QGP radiation in different invariant-mass regions, one can probe different stages during the time evolution of the QGP phase.

The measurements of the above dileptons require large detector acceptance, large event statistics, and clean lepton identification. STAR collected a large sample of Au + Au collision events with the TOF detector. The TOF detector greatly extended the capability of the STAR experiment for particle identification. Combining the timing measurement from the TOF detector, and the momentum and ionization energy loss (dE/dx) measurements from the tracking detector, namely, the time projection chamber (TPC), one can cleanly identify low-momentum electrons with high efficiency and purity. Figure 3a shows the nσ_e (the n times of the standard deviation of measured dE/dx to the Bichsel prediction) as a function of particle momentum. The electron band largely overlapped with charged hadrons when using data from the TPC alone. With a TOF velocity close to the speed of light in vacuum, most of the hadrons were rejected. The remaining hadrons were a clean electron band and fast hadrons, as shown in Figure 3b.

The wide, uniform pseudorapidity and azimuthal acceptance of the STAR TPC and TOF detector allow for the precision reconstruction of dielectron pairs with the good systematic control of uncorrelated and correlated backgrounds. After the removal of these background contributions, dielectron invariant-mass spectra were measured with STAR at various collision energy levels. Decays from light mesons after a freeze-out (usually

called a cocktail) can be removed by simulating the cocktail contributions. The remaining dielectron spectra are of particular interest and expected to contain radiation information from various stages of heavy-ion collisions before freeze-out.

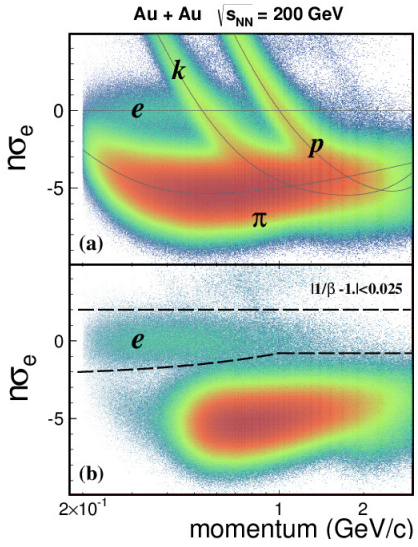

Figure 3. (**a**) nσ_e measured with the time projection chamber in Au + Au collisions at $\sqrt{s_{NN}}$ = 200 GeV. (**b**) nσ_e with a particle velocity cut using the TOF detector. The figure was taken from [72].

Figure 4 shows e^+e^- invariant-mass spectra after cocktail subtraction in Au + Au collisions at $\sqrt{s_{NN}}$ = 27, 39, 62.4, and 200 GeV [73,74]. The figure shows model calculations for total thermal radiation (solid lines), including both in-medium hadronic (dashed lines) and QGP (dotted lines) contributions. The model calculations provide a consistent description of the measured dielectron spectra across broad-energy and invariant-mass regions. In the LMR, the dominant hadronic radiation is mainly generated through ρ meson in-medium broadening through interactions with the hadronic medium, particularly baryons. The same model also provided a consistent description of the invariant-mass spectrum of the dimuon pairs measured in the NA60 experiment at SPS [75]. The ρ meson in-medium broadening was suggested to be evidence of the partial restoration of the chiral symmetry in the hot QCD medium [76]. The QGP radiation contribution was expected to take over at the IMR, where the precision of the current measurements is limited. The search and investigation of the QGP thermal radiation are future directions in the dilepton programs at both RHIC and LHC.

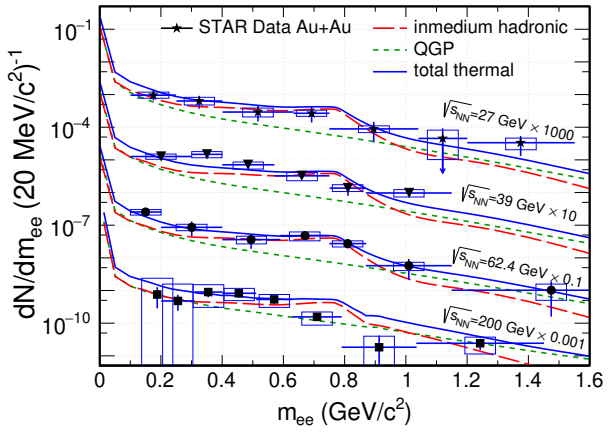

Figure 4. STAR measurements of dielectron invariant-mass spectra after cocktail removal in Au + Au collisions at $\sqrt{s_{NN}}$ = 27, 39, 62.4, and 200 GeV [73,74] in comparison with the model calculations of the total thermal radiation (blue solid lines), including in-medium hadronic (red dashed lines) and QGP (green dotted lines) contributions [10,71,77].

Figure 5 shows the collision energy dependence of the integrated dielectron yield, normalized to the charge pion dN/dy in the low-mass region of $0.3 < M_{ll} < 0.7$ GeV/c^2 measured from HADES [78], NA60 [75], and STAR [73,74]. Theoretical model calculations on dielectron yields (dashed blue line) and the fireball lifetime (solid red line) are also shown in the figure. The model provides a good description of the energy dependence, which exhibited a modest increase from the SPS to the top RHIC energy. This increase also shows the good tracking of the fireball lifetime across a broad collision energy range. The measurements from STAR shown here are from the Beam Energy Scan (BES) Phase I. The recorded BES-II data and analyses further extend the measurements from 19.6 GeV down to 7.7 GeV, offering new insights of the hot medium properties in the high-baryon-density region. Future experiments, such as NA60+, CBM and MPD, could further extend the measurements to low energy [79–81].

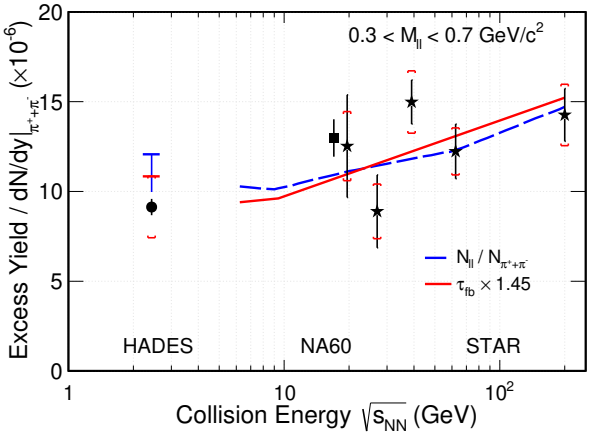

Figure 5. Collision energy dependence of the integrated dielectron yield normalized to the charged pion dN/dy in the low-mass region of $0.3 < M_{ll} < 0.7$ GeV/c^2 measured from HADES [78], NA60 [75] and STAR [73,74] in comparison with the model calculations of dielectron yields (dashed blue line) and the fireball lifetime (solid red line) [77].

4. Dileptons from the Breit–Wheeler Process

When matter and antimatter [82] interact in a process called annihilation, they both disappear, and their mass is instantly converted into energy [83,84]. In 1934, Breit and Wheeler started the theoretical study of the simplest reverse process of the collision of two light quanta ($\gamma\gamma \rightarrow e^+e^-$) to create mass from energy [85]. The Breit–Wheeler study indicated that it is impossible to achieve this process via γ-ray collisions in existing Earth base experiments, which still holds true. Alternatively, they proposed observing the process via relativistic heavy-ion collisions in which the highly Lorentz-contracted electromagnetic field induced by fast-moving ions can be treated as a powerful source of photons for collisions. The treatment of quantizing the Lorentz-boosted Coulomb field was first proposed by Fermi [86], and further developed by Williams and Weizsacker [13], which is called the Williams–Weizsacker method or equivalent photon approximation (EPA).

Over the past few decades, dielectron production from the collision of light quanta was observed at various hadron and electron–positron collider experiments [19,25–27,29,87–92]. However, the existing experimental results lack precision and differential measurements to demonstrate themselves as the Breit–Wheeler process. The pioneering study of the Breit–Wheeler process at RHIC was conducted by STAR with Au + Au collision data from $\sqrt{s_{\rm NN}}$ = 200 GeV taken in 2001 [25]. The data were collected with the trigger of ultraperipheral collisions (UPCs) in order to reject hadronic interactions. The specific energy loss (dE/dx) from the TPC only allows for the identification of electrons from pion backgrounds in a very limited kinematic range ($65 < p_T < 130$ MeV/c). In total, 52 candidate events were selected out of 800,000 triggered events in which the limited statistics prevents further claims from being made. For the data taken in 2010 with the

fully installed TOF, the contamination background from hadron pairs could be largely reduced by using the double difference in the time of flight between the two measured tracks, and the expectation for dielectrons calculated using the measured momentum and path length from the TPC. Together with dE/dx information from the TPC, the optimized section criteria could ensure a 99% purity of dielectron candidates.

Measurements of the production rate of exclusive dielectron pairs from the data taken in 2010 [93] are shown in Figure 6. The measurements were performed in the fiducial phase space reported in the figure. Figure 6a shows the invariant-mass spectrum of exclusive dielectron pairs, which was smooth and featureless. The potential background contribution from exclusive vector meson photoproduction with the decay branch of dielectrons was estimated with STARLight [94] model and is shown as solid purple lines in the figure; the results were negligible in comparison with the experimental data. Figure 6b displays the differential $|\cos\theta'|$ distribution in which θ' is defined as the polar angle of the electron (positron) with respect to the beam in the electron–positron center-of-mass frame. The falloff of the distribution resulted from the detector acceptance. In comparison with isotropic emission (dashed line in the figure), the measured exclusive process exhibited enhancement toward a small polar angle. The differential cross-section, as a function of the pair transverse momentum ($P_\perp$), is shown in Figure 6c. The data characterize a clear peak in the production rate at very low transverse momentum. All these features were the consequence of the energy spectrum and quantum numbers of the two photons involved in the Breit–Wheeler process. Therefore, the Breit–Wheeler process was unambiguously identified for relativistic heavy-ion collisions in this measurement.

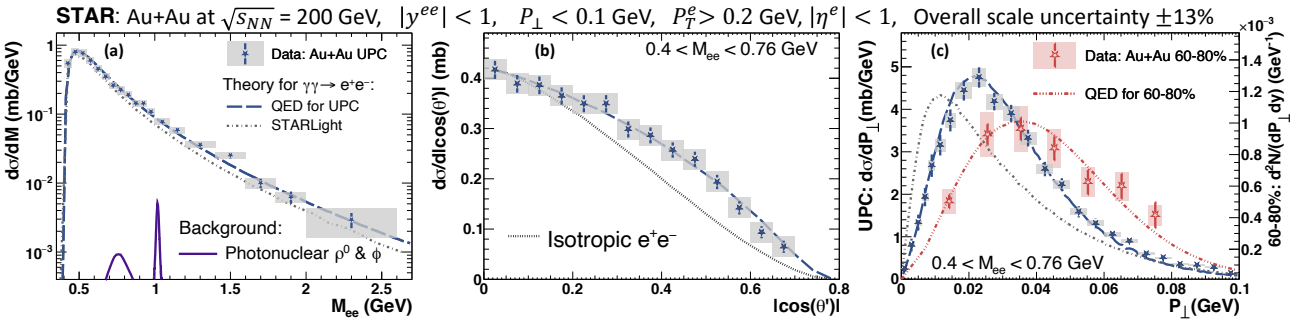

Figure 6. Differential cross-sections for exclusively dielectron pairs as functions of (**a**) invariant-mass M_{ee} (and potential vector-meson background from photoproduction), (**b**) polar angle distribution $|\cos\theta'|$, and (**c**) pair transverse momentum $P_\perp$. The figure was taken from [93].

Conventionally, the Breit–Wheeler process is only studied in UPCs to reject hadronic backgrounds. Furthermore, photon-induced processes are not generally considered to add up coherently for collisions with nuclear overlap. This begins with J/ψ measurements at a very low transverse momentum in Pb + Pb collisions from ALICE [28], in which significant excesses were observed in peripheral collisions. The abnormal excesses of J/ψ were confirmed via the STAR measurements [95], and well-described by the phenomenological model with a coherent photon-nucleus production mechanism [50,96–99]. Assuming that coherent photon nuclear production is responsible for the observed J/ψ excesses, the Breit–Wheeler process should also exist and contribute to dielectron production for collisions with nuclear overlap.

Utilizing the datasets collected in 2010, 2011, and 2012, STAR performed dielectron measurements at a low transverse momentum for hadronic heavy-ion collisions (non-UPCs) [38]. The electron identification criteria were the same as those described in Section 3. Figure 7 shows the transverse momentum distributions of dielectron pairs in different mass regions for 60–80% Au + Au and U + U collisions. As expected, a significant excess was observed and concentrated below $p_T \sim 0.15$ GeV/c with respect to the hadronic cocktail. The magnitude of the excess could be well-described with the model incorporated with the Breit–Wheeler process in hadronic heavy-ion collisions [100]. To further investigate the

features of the Breit–Wheeler process in hadronic heavy-ion collisions, STAR measured the p_T^2 distributions of excess yields within acceptance in different mass regions for peripheral collisions, as shown in Figure 8. The aforementioned model calculations are also plotted in the figure. The theoretical results fell below the data points at large p_T^2 values, and overshot the data at low p_T^2. Such a discrepancy can be well-quantified by the corresponding $\sqrt{\langle p_T^2 \rangle}$ of p_T^2 distributions, as shown in Figure 8d. The disagreement between the data and the model calculations suggests the possible origins of the p_T broadening from the hot medium created in the nuclear overlap region. By introducing a magnetic field trapped in an electrically conducting QGP, the p_T broadening can be reasonably described. ATLAS collaboration also found a significant p_T broadening effect via the dimuon channel in comparison to those in UPCs [39], and quantified the effect via the acoplanarity of dimuon pairs. Alternatively, the broadening was explained by the electromagnetic scattering of leptons in the hot and dense medium [40]. All these descriptions of the broadening effect assumed that there was no impact-parameter dependence of the p_T distribution in the production process. Recent theoretical calculations [30,31] that recovered the impact parameter dependence demonstrated that the broadening was mainly from the initial light quantum collisions. This was further experimentally confirmed via CMS measurements [34] through exclusive dimuon production from photon–photon collisions in UPCs. Small tension still existed between data and theoretical calculations, which left room for possible effects from the hot medium.

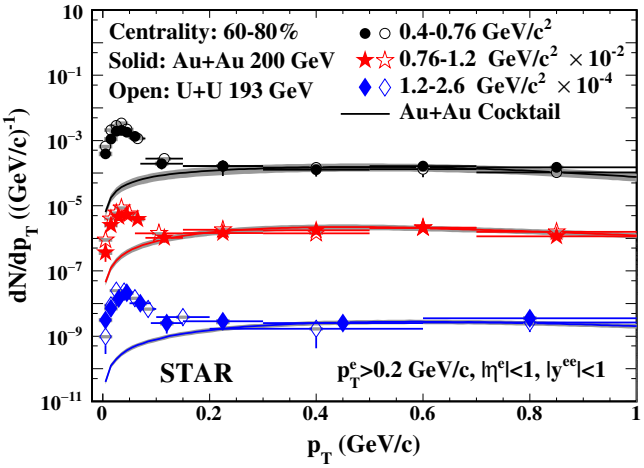

Figure 7. The transverse momentum distributions of dielectron pairs within STAR acceptance for different mass regions in peripheral Au + Au and U + U collisions compared to the hadronic cocktail. The figure was taken from [38].

Due to the extreme Lorentz contraction in relativistic heavy-ion collisions, the induced electromagnetic field was almost fully perpendicular to the direction of motion of the heavy nuclei, suggesting that the induced photons were fully linearly polarized in the transverse plane. Li et al. [101] proposed that the collisions of linearly polarized photons can lead to second- and fourth-order modulations in the azimuth (in the plane perpendicular to the beam direction). As shown in Figure 9, STAR performed the first measurement of the decay angular distribution ($\Delta\phi$) for the Breit–Wheeler process in relativistic heavy-ion collisions. Significant $\cos(4\Delta\phi)$ modulation was found, which could be described well via the numerical lowest-order QED calculation [102]. The observed angular modulation was closely related to the vacuum birefringence in which the vacuum was polarized by the extremely strong electromagnetic field in the absence of a medium [103]. This also inspired the discovery of $\cos(2\Delta\phi)$ modulation for vector meson photoproduction [45,48,51] in heavy-ion collisions.

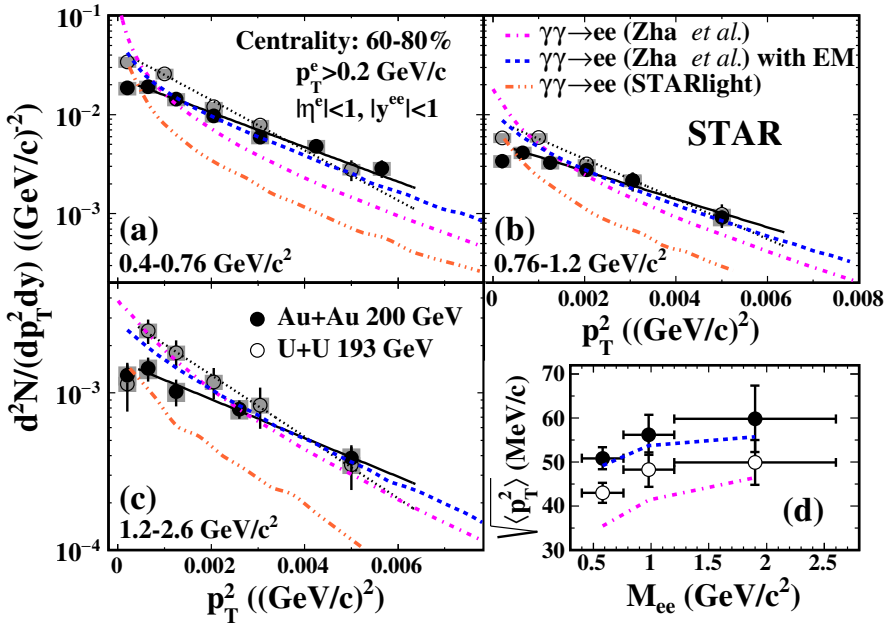

Figure 8. The p_T^2 distributions of excess yields within the STAR fiducial cuts in mass regions of (**a**) 0.40–0.76, (**b**) 0.76–1.2, and (**c**) 1.2–2.6 GeV/c^2 for peripheral Au + Au and U + U collisions. (**d**) The corresponding $\sqrt{\langle p_T^2 \rangle}$ of p_T^2 distributions. The figure was taken from [38].

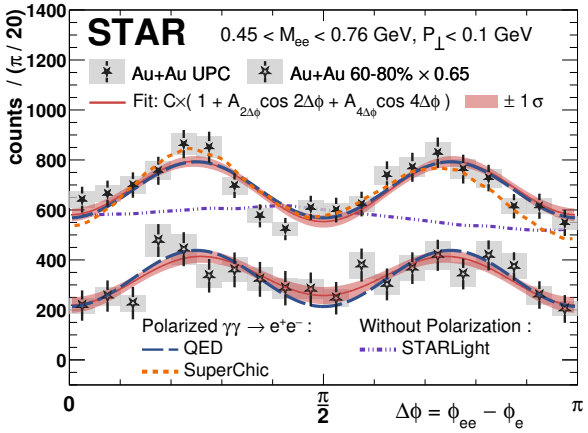

Figure 9. Decay angular distribution from UPCs and 60–80% central collisions with the theoretical calculations from QED [101], STARLight [94], and SUPERCHIC3 [104]. The figure was taken from [93].

5. Future Perspectives

The dilepton measurements at SPS with NA60 in the dimuon channel were performed with high statistics and with high data quality almost two decades ago. RHIC could provide important insights in the dielectron channel at the top energy and in the Beam Energy Scan Phase I (BES-I). The high-statistics data from BES-II and future data at the top energy level showed potential for providing the temperature measurements around the phase boundary and at the QGP phase. Future ALICE upgrades and experiments at high baryon density also promise an exciting dilepton program with LHC energies [79–81,105].

The future data-taking plan at RHIC and the LHC would provide an opportunity to perform the high-precision multidifferential analysis of these two photon-related physics [106,107]. The incoming RHIC run would allow for STAR to significantly improve the precision of the transverse momentum spectra and the angular modulation strength for the Breit–Wheeler process. The improved precision of transverse momentum spectra provides an additional powerful constraint to the proposed final-state broadening effects. The added precision

in the angular modulation measurements is expected to experimentally demonstrate the impact parameter dependence of angular modulation strength, which is predicated by lowest-order QED calculations. Furthermore, precise angular modulation measurements could also serve as a sensitive probe of the hot medium, since the final state interactions would destroy the angular modulation resulting from the linear polarization of the initial photons. The much larger statistics provided by the future data-taking plan makes more differential measurements, such as angular modulation strength versus pair transverse momentum for dielectrons from the Breit–Wheeler process possible. The data-taking campaigns planned at the LHC would also allow for ALICE to measure the Breit–Wheeler process with much more precise measurements in a similar region of phase space as that measured at RHIC, but in collisions with a much larger Lorentz boost factor. Such measurements provide additional information on the photon kinematic distributions over a broad range of photon energy. Similarly, analyses of the $\gamma\gamma \rightarrow \mu^+\mu^-$ process in events with a hadronic overlap by CMS and ATLAS [107,108] from the future data-taking plan would shed new light on the presence (or lack) of medium-induced modifications. In much of the progress achieved in the last decade, TOF played an indispensable role. We anticipate that future progresses on this subject would continue to rely on the time-of-flight detector with its revolutionary technology advances.

Author Contributions: All authors contributed equally. All authors have read and agreed to the published version of the manuscript.

Funding: This review article received no external funding.

Data Availability Statement: The STAR published data are available at the STAR publication webpage: https://drupal.star.bnl.gov/STAR/publications (accessed on 27 December 2022) and HEPData: https://www.hepdata.net/ (accessed on 27 December 2022).

Conflicts of Interest: The authors declare no conflict of interest.

References

1. Bazavov, A.; Ding, H.T.; Hegde, P.; Kaczmarek, O.; Karsch, F.; Karthik, N.; Laermann, E.; Lahiri, A.; Larsen, R.; Li, S.T.; et al. Chiral crossover in QCD at zero and non-zero chemical potentials. *Phys. Lett. B* **2019**, *795*, 15–21.
2. Borsanyi, S.; Fodor, Z.; Guenther, J.N.; Kara, R.; Katz, S.D.; Parotto, P.; Pasztor, A.; Ratti, C.; Szabo, K.K. QCD Crossover at Finite Chemical Potential from Lattice Simulations. *Phys. Rev. Lett.* **2020**, *125*, 052001, [CrossRef] [PubMed]
3. Braun-Munzinger, P.; Koch, V.; Schäfer, T.; Stachel, J. Properties of hot and dense matter from relativistic heavy ion collisions. *Phys. Rept.* **2016**, *621*, 76–126. [CrossRef]
4. Busza, W.; Rajagopal, K.; van der Schee, W. Heavy Ion Collisions: The Big Picture, and the Big Questions. *Ann. Rev. Nucl. Part. Sci.* **2018**, *68*, 339–376. [CrossRef]
5. Shuryak, E.V. Quark-Gluon Plasma and Hadronic Production of Leptons, Photons and Psions. *Phys. Lett. B* **1978**, *78*, 150 [CrossRef]
6. McLerran, L.D.; Toimela, T. Photon and Dilepton Emission from the Quark - Gluon Plasma: Some General Considerations. *Phys. Rev. D* **1985**, *31*, 545 [CrossRef] [PubMed]
7. Shuryak, E.V.; Xiong, L. Dilepton and photon production in the 'hot glue' scenario. *Phys. Rev. Lett.* **1993**, *70*, 2241–2244. [CrossRef]
8. Adamczewski-Musch, J.; Arnold, O.; Behnke, C.; Belounnas, A.; Belyaev, A.; Berger-Chen, J.C.; Biernat, J.; Blanco, A.; Blume, C.; Böhmer, M.; et al. Probing dense baryon-rich matter with virtual photons. *Nat. Phys.* **2019**, *15*, 1040–1045 [CrossRef]
9. van Hees, H.; Rapp, R. Comprehensive interpretation of thermal dileptons at the SPS. *Phys. Rev. Lett.* **2006**, *97*, 102301, [CrossRef]
10. Rapp, R.; van Hees, H. Thermal Dileptons as Fireball Thermometer and Chronometer. *Phys. Lett. B* **2016**, *753*, 586–590. [CrossRef]
11. Shen, C.; Heinz, U.W.; Paquet, J.F.; Gale, C. Thermal photons as a quark-gluon plasma thermometer reexamined. *Phys. Rev. C* **2014**, *89*, 044910. [CrossRef]
12. Toll, J.S. The Dispersion Relation for Light and Its Application to Problems Involving Electron Pairs. Ph.D. Thesis, Princeton University, Princeton, NJ, USA, 1952.
13. Williams, E.J. Nature of the High Energy Particles of Penetrating Radiation and Status of Ionization and Radiation Formulae. *Phys. Rev.* **1934**, *45*, 729–730 [CrossRef]
14. Eichler, J. Theory of relativistic ion-atom collisions. *Phys. Rep.* **1990**, *193*, 165–277 [CrossRef]
15. Baur, G. Multiple electron-positron pair production in relativistic heavy-ion collisions: A strong-field effect. *Phys. Rev. A* **1990**, *42*, 5736–5738 [CrossRef]
16. Baltz, A.J.; Gelis, F.; McLerran, L.; Peshier, A. Coulomb corrections to e^+e^- production in ultra-relativistic nuclear collisions. *Nucl. Phys. A* **2001**, *695*, 395–429 [CrossRef]

17. Belkacem, A.; Gould, H.; Feinberg, B.; Bossingham, R.; Meyerhof, W.E. Capture, ionization, and pair-production processes in relativistic heavy-ion collisions in the 1-GeV/nucleon energy range. *Phys. Rev. A* **1997**, *56*, 2806–2818 [CrossRef]
18. Belkacem, A.; Claytor, N.; Dinneen, T.; Feinberg, B.; Gould, H. Electron capture from pair production by Au^{79+} at 10.8 GeV/nucleon. *Phys. Rev. A* **1998**, *58*, 1253–1255 [CrossRef]
19. Vane, C.R.; Datz, S.; Dittner, P.F.; Krause, H.F.; Bottcher, C.; Strayer, M.; Schuch, R.; Gao, H.; Hutton, R. Electron-positron pair production in Coulomb collisions of ultrarelativistic sulfur ions with fixed targets. *Phys. Rev. Lett.* **1992**, *69*, 1911–1914 [CrossRef]
20. Arsene, I.; Bearden, I.G.; Beavis, D.; Besliu, C.; Budick, B.; Bøggild, H.; Chasman, C.; Christensen, C.H.; Christiansen, P.; Cibor, J.; et al. Quark–gluon plasma and color glass condensate at RHIC? The perspective from the BRAHMS experiment. *Nucl. Phys. A* **2005**, *757*, 1–27. [CrossRef]
21. Back, B.B.; Baker, M.D.; Ballintijn, M.; Barton, D.S.; Becker, B.; Betts, R.R.; Bickley, A.A.; Bindel, R.; Budzanowski, A.; Busza, W.; et al. The PHOBOS perspective on discoveries at RHIC. *Nucl. Phys. A* **2005**, *757*, 28–101. [CrossRef]
22. Adams, J.; Aggarwal, M.M.; Ahammed, Z.; Amonett, J.; Anderson, B.D.; Arkhipkin, D.; Averichev, G.S.; Badyal, S.K.; Bai, Y.; Balewski, J.; et al. Experimental and theoretical challenges in the search for the quark–gluon plasma: The STAR Collaboration's critical assessment of the evidence from RHIC collisions. *Nucl. Phys. A* **2005**, *757*, 102–183. [CrossRef]
23. Adcox, K.; Adler, S.S.; Afanasiev, S.; Aidala, C.; Ajitan, N.N.; Akiba, Y.; Al-Jamel, A.; Alexer, J.; Amirikas, R.; Aoki, K.; et al. Formation of dense partonic matter in relativistic nucleus–nucleus collisions at RHIC: Experimental evaluation by the PHENIX Collaboration. *Nucl. Phys. A* **2005**, *757*, 184–283. [CrossRef]
24. Fatyga, M.; Rhoades-Brown, M.; Tannenbaum, M. *Can RHIC Be Used to Test QED?* Technical Report; Brookhaven National Lab.: Upton, NY, USA, 1990.
25. Adams, J.; Aggarwal, M.M.; Ahammed, Z.; Amonett, J.; Anderson, B.D.; Arkhipkin, D.; Averichev, G.S.; Bai, Y.; Balewski, J.; Barannikova, O.; et al. Production of e^+e^- pairs accompanied by nuclear dissociation in ultraperipheral heavy-ion collisions. *Phys. Rev. C* **2004**, *70*, 031902 [CrossRef]
26. Drachenberg, J.L.; Hagiwara, M.N.; Isenhower, D.; Isenhower, L.; Omiwade, O.O.; Smith, W.C.; Towell, R.S.; Singh, C.P.; Singh, V.; Tuli, S.K.; et al. Photoproduction of J/ψ and of high mass e^+e^- in ultra-peripheral Au+Au collisions at $\sqrt{s_{\rm NN}} = 200$ GeV. *Phys. Lett. B* **2009**, *679*, 321–329. [CrossRef]
27. Abbas, E.; Abelev, B.; Adam, J.; Adamová, D.; Adare, A.M.; Aggarwal, M.M.; Aglieri Rinella, G.; Agnello, M.; Agocs, A.G.; Agostinelli, A.; et al. Charmonium and e^+e^- pair photoproduction at mid-rapidity in ultra-peripheral Pb-Pb collisions at $\sqrt{s_{\rm NN}} = 2.76$ TeV. *Eur. Phys. J. C* **2013**, *73*, 2617. [CrossRef] [PubMed]
28. Adam, J.; Adamová, D.; Aggarwal, M.M.; Rinella, G.A.; Agnello, M.; Agrawal, N.; Ahammed, Z.; Ahn, S.U.; Aiola, S.; Akindinov, A.; et al. Measurement of an excess in the yield of J/ψ at very low $p_{\rm T}$ in Pb-Pb collisions at $\sqrt{s_{\rm NN}} = 2.76$ TeV. *Phys. Rev. Lett.* **2016**, *116*, 222301. [CrossRef]
29. Barreiro Alonso, F.; Aad, G.; Arnal, V.; Cantero, J.; De la Torre, H.; Del Peso, J.; Glasman, C.; Llorente, Merino, J.; Terrón, J., ATLAS Collaboration. Measurement of exclusive $\gamma\gamma \to l^+l^-$ production in proton–proton collisions at $\sqrt{s} = 7$ TeV with the ATLAS detector. *Phys. Lett. B* **2015**, *749*, 242–261. [CrossRef]
30. Zha, W.; Brandenburg, J.D.; Tang, Z.; Xu, Z. Initial transverse-momentum broadening of Breit-Wheeler process in relativistic heavy-ion collisions. *Phys. Lett. B* **2020**, *800*, 135089. [CrossRef]
31. Wang, R.j.; Pu, S.; Wang, Q. Lepton pair production in ultraperipheral collisions. *Phys. Rev. D* **2021**, *104*, 056011. [CrossRef]
32. Klein, S.; Mueller, A.H.; Xiao, B.W.; Yuan, F. Lepton Pair Production Through Two Photon Process in Heavy Ion Collisions. *Phys. Rev. D* **2020**, *102*, 094013. [CrossRef]
33. Kłusek-Gawenda, M.; Schäfer, W.; Szczurek, A. Centrality dependence of dilepton production via $\gamma\gamma$ processes from Wigner distributions of photons in nuclei. *Phys. Lett. B* **2021**, *814*, 136114. [CrossRef]
34. Sirunyan, A.M.; Tumasyan, A.; Adam, W.; Bergauer, T.; Dragicevic, M.; Erö, J.; Del Valle, A.E.; Fruehwirth, R.; Jeitler, M.; Krammer, N.; et al. Observation of Forward Neutron Multiplicity Dependence of Dimuon Acoplanarity in Ultraperipheral Pb-Pb Collisions at $\sqrt{s_{NN}} = 5.02$ TeV. *Phys. Rev. Lett.* **2021**, *127*, 122001. [CrossRef] [PubMed]
35. Sun, Z.H.; Zheng, D.X.; Zhou, J.; Zhou, Y.J. Studying Coulomb correction at EIC and EicC. *Phys. Lett. B* **2020**, *808*, 135679. [CrossRef]
36. Zha, W.; Tang, Z. Discovery of higher-order quantum electrodynamics effect for the vacuum pair production. *J. High Energy Phys.* **2021**, *2021*, 83. [CrossRef]
37. Brandenburg, J.D.; Zha, W.; Xu, Z. Mapping the electromagnetic fields of heavy-ion collisions with the Breit-Wheeler process. *Eur. Phys. J. A* **2021**, *57*, 299. [CrossRef]
38. STAR Collaboration; Adam, J. Low-p_T e^+e^- Pair Production in Au+Au Collisions at $\sqrt{s_{\rm NN}} = 200$ GeV and U+U Collisions at $\sqrt{s_{\rm NN}} = 193$ GeV at STAR. *Phys. Rev. Lett.* **2018**, *121*, 132301. [CrossRef]
39. Aaboud, M.; Aad, G.; Abbott, B.; Abeloos, B.; Abhayasinghe, D.K.; Abidi, S.H.; AbouZeid, O.S.; Abraham, N.L.; Abramowicz, H.; Abreu, H.; et al. Observation of Centrality-Dependent Acoplanarity for Muon Pairs Produced via Two-Photon Scattering in Pb + Pb Collisions at $\sqrt{s_{\rm NN}} = 5.02$ TeV with the ATLAS Detector. *Phys. Rev. Lett.* **2018**, *121*, 212301. [CrossRef]
40. Klein, S.; Mueller, A.H.; Xiao, B.W.; Yuan, F. Acoplanarity of a Lepton Pair to Probe the Electromagnetic Property of Quark Matter. *Phys. Rev. Lett.* **2019**, *122*, 132301. [CrossRef]
41. Wang, Z.; Zhao, J.; Greiner, C.; Xu, Z.; Zhuang, P. Incomplete electromagnetic response of hot QCD matter. *Phys. Rev. C* **2022**, *105*, L041901. [CrossRef]

42. An X.; Bluhm, M.; Du, L.; Dunne, G.V.; Elfner, H.; Gale, C.; Grefa, J.; Heinz, U.; Huang, A.; Karthein, J.M.; et al. The BEST framework for the search for the QCD critical point and the chiral magnetic effect. *Nucl. Phys. A* **2022**, *1017*, 122343. [CrossRef]
43. Kłusek-Gawenda, M.; Rapp, R.; Schäfer, W.; Szczurek, A. Dilepton Radiation in Heavy-Ion Collisions at Small Transverse Momentum. *Phys. Lett. B* **2019**, *790*, 339–344. [CrossRef]
44. Wang, X.; Brandenburg, J.D.; Ruan, L.; Shao, F.; Xu, Z.; Yang, C.; Zha, W. Energy Dependence of the Breit-Wheeler process in Heavy-Ion Collisions and its Application to Nuclear Charge Radius Measurements. *arXiv* **2022**, arXiv:2207.05595.
45. Abdallah, M.S.; Aboona, B.E.; Adam, J.; Adamczyk, L.; Adams, J.R.; Adkins, J.K.; Agakishiev, G.; Aggarwal, I.; Aggarwal, M.M.; Ahammed, Z.; et al. Tomography of Ultra-relativistic Nuclei with Polarized Photon-gluon Collisions. *arXiv* **2022**, arXiv:2204.01625.
46. Budker, D.; Berengut, J.C.; Flambaum, V.V.; Gorchtein, M.; Jin, J.; Karbstein, F.; Krasny, M.W.; Litvinov, Y.A.; Pálffy, A.; Pascalutsa, V.; et al. Expanding Nuclear Physics Horizons with the Gamma Factory. *Ann. Phys.* **2021**, *534*, 2100284. [CrossRef]
47. Hatta, Y.; Xiao, B.W.; Yuan, F.; Zhou, J. Azimuthal angular asymmetry of soft gluon radiation in jet production. *Phys. Rev. D* **2021**, *104*, 054037. [CrossRef]
48. Xing, H.; Zhang, C.; Zhou, J.; Zhou, Y.J. The $\cos 2\phi$ azimuthal asymmetry in ρ^0 meson production in ultraperipheral heavy ion collisions. *JHEP* **2020**, *10*, 064. [CrossRef]
49. Bor, J.; Boer, D. TMD Evolution Study of the $\cos 2\phi$ Azimuthal Asymmetry in Unpolarized J/ψ Production at EIC. *arXiv* **2022**, arXiv:hep-ph/2204.01527.
50. Zha, W.; Ruan, L.; Tang, Z.; Xu, Z.; Yang, S. Double-slit experiment at fermi scale: Coherent photoproduction in heavy-ion collisions. *Phys. Rev. C* **2019**, *99*, 061901. [CrossRef]
51. Zha, W.; Brandenburg, J.D.; Ruan, L.; Tang, Z.; Xu, Z. Exploring the double-slit interference with linearly polarized photons. *Phys. Rev. D* **2021**, *103*, 033007. [CrossRef]
52. Dyndal, M.; Klusek-Gawenda, M.; Schott, M.; Szczurek, A. Anomalous electromagnetic moments of τ lepton in $\gamma\gamma \to \tau^+\tau^-$ reaction in Pb+Pb collisions at the LHC. *Phys. Lett. B* **2020**, *809*, 135682. [CrossRef]
53. Xu, I.; Lewis, N.; Wang, X.; Brandenburg, J.D.; Ruan, L. Search for Dark Photons in $\gamma\gamma \to e^+e^-$ at RHIC. *arXiv* **2022**, arXiv:2211.02132.
54. Cerron Zeballos, E.; Crotty, I.; Hatzifotiadou, D.; Lamas Valverde, J.; Neupane, S.; Williams, M.C.S.; Zichichi, A. A New type of resistive plate chamber: The Multigap RPC. *Nucl. Instrum. Meth. A* **1996**, *374*, 132–136. [CrossRef]
55. Li, C.; Wu, J.; Wang, X.; Chen, H.; Xu, Z.; Shao, M.; Ye, S.; Ruan, L.; Huang, S. A high time resolution multi-gap resistive plate chamber. *Nucl. Sci. Tech.* **2002**, *13*, 6–10.
56. Li, C.; Wu, J.; Chen, H.; Wang, X.; Xu, Z.; Wang, Z.; Shao, M.; Huang, S.; Ruan, L. A prototype of the high time resolution MRPC. *Chin. Phys. C* **2001**, *25*, 933–935.
57. Shao, M.; Ruan, L.J.; Chen, H.F.; Wu, J.; Li, C.; Xu, Z.Z.; Wang, X.L.; Huang, S.L.; Wang, Z.M.; Zhang, Z.P. Beam test results of two kinds of multi-gap resistive plate. *Nucl. Instrum. Meth. A* **2002**, *492*, 344–350. [CrossRef]
58. Wu, J.; Bonner, B.; Chen, H.F.; Dong, X.; Eppley, G.; Geurts, F.; Huang, S.L.; Li, C.; Llope, W.J.; Nussbaum, T.; et al. The performance of the TOFr tray in STAR. *Nucl. Instrum. Meth. A* **2005**, *538*, 243–248. [CrossRef]
59. Geurts, F.; Shao, M.; Bonner, B.; Chen, H.; Dong, X.; Eppley, G.; Huang, S.; Li, C.; Li, J.; Llope, W.; et al. Performance of the prototype MRPC detector for STAR. *Nucl. Instrum. Meth. A* **2004**, *533*, 60–64. [CrossRef]
60. Shao, M.; Barannikova, O.Y.; Dong, X.; Fisyak, Y.; Ruan, L.; Sorensen, P.; Xu, Z. Extensive particle identification with TPC and TOF at the STAR experiment. *Nucl. Instrum. Meth. A* **2006**, *558*, 419–429. [CrossRef]
61. Adams, J.; Aggarwal, M.M.; Ahammed, Z.; Amonett, J.; Anderson, B.D.; Arkhipkin, D.; Averichev, G.S.; Badyal, S.K.; Bai, Y.; Balewski, J.; et al. Pion, kaon, proton and anti-proton transverse momentum distributions from $p + p$ and $d +$ Au collisions at $\sqrt{s_{\rm NN}} = 200$ GeV. *Phys. Lett. B* **2005**, *616*, 8–16. [CrossRef]
62. Adams, J.; Aggarwal, M.M.; Ahammed, Z.; Amonett, J.; Anderson, B.D.; Arkhipkin, D.; Averichev, G.S.; Badyal, S.K.; Bai, Y.; Balewski, J.; et al. Open charm yields in $d +$ Au collisions at $\sqrt{s_{\rm NN}} = 200$ GeV. *Phys. Rev. Lett.* **2005**, *94*, 062301. [CrossRef]
63. Ruan, L.; Shao, M.; Chen, H.; Li, C.; Wang, X.; Wu, J.; Xu, Z.; Huang, S. A Monte Carlo Simulation of Multi-gap Resistive Plate Chamber and Comparison with Experimental Results. *Chin. Phys. C* **2003**, *27*, 712–715.
64. Zhao, Y.E.; Wang, X.L.; Liu, H.D.; Chen, H.F.; Li, C.; Wu, J.; Xu, Z.Z.; Shao, M.; Zeng, H.; Zhou, Y.; et al. Effect of temperature on the multi-gap resistive plate chamber operation. *Nucl. Instrum. Meth. A* **2005**, *547*, 334–341. [CrossRef]
65. Shao, M.; Zhao, Y.; Li, C.; Chen, H.F.; Wang, X.L.; Wu, J.; Sun, Y.J.; Ruan, L.J. Simulation study on the operation of a multi-gap resistive plate chamber. *Measur. Sci. Tech.* **2006**, *17*, 123–127. [CrossRef]
66. Shao, M.; Dong, X.; Tang, Z.; Xu, Y.; Huang, M.; Li, C.; Chen, H.F.; Lu, Y.; Zhang, Y. Upgrade of the calibration procedure for a STAR time-of-flight detector with new electronics. *Measur. Sci. Tech.* **2009**, *20*, 025102. [CrossRef]
67. Zou, T.; Wang, X.; Shao, M.; Sun, Y.; Zhao, Y.E.; Tang, H.; Ming, Y.; Guo, J.; Zhang, Y.; Li, C.; et al. Quality control of MRPC mass production for STAR TOF. *Nucl. Instrum. Meth. A* **2009**, *605*, 282–292. [CrossRef]
68. Llope, W.J. Multigap RPCs in the STAR experiment at RHIC. *Nucl. Instrum. Meth. A* **2012**, *661*, S110–S113. [CrossRef]
69. Shao, M.; Sun, Y.; Tang, Z.; Zhang, Y.; Zhang, Y.; Zhang, Z.; Zhao, L. Technology Development for Nuclear Physics at USTC. *Nucl. Phys. News* **2019**, *29*, 5–11. [CrossRef]
70. Hohler, P.M.; Rapp, R. Is ρ-Meson Melting Compatible with Chiral Restoration? *Phys. Lett. B* **2014**, *731*, 103–109. [CrossRef]
71. Rapp, R.; Wambach, J. Low mass dileptons at the CERN SPS: Evidence for chiral restoration? *Eur. Phys. J. A* **1999**, *6*, 415–420. [CrossRef]

72. Adamczyk, L.; Adkins, J.K.; Agakishiev, G.; Aggarwal, M.M.; Ahammed, Z.; Alekseev, I.; Alford, J.; Aparin, A.; Arkhipkin, D.; Aschenauer, E.C.; et al. Measurements of Dielectron Production in Au+Au Collisions at $\sqrt{s_{\rm NN}}$ = 200 GeV from the STAR Experiment. *Phys. Rev. C* **2015**, *92*, 024912. [CrossRef]
73. Adamczyk, L.; Adkins, J.K.; Agakishiev, G.; Aggarwal, M.M.; Ahammed, Z.; Alekseev, I.; Alford, J.; Aparin, A.; Arkhipkin, D.; Aschenauer, E.C.; et al. Energy dependence of acceptance-corrected dielectron excess mass spectrum at mid-rapidity in Au+Au collisions at $\sqrt{s_{\rm NN}} = 19.6$ and 200 GeV. *Phys. Lett. B* **2015**, *750*, 64–71. [CrossRef]
74. Adam, J.; Adamczyk, L.; Adams, J.R.; Adkins, J.K.; Agakishiev, G.; Aggarwal, M.; Ahammed, Z.; Alekseev, I.; Anderson, D.M.; Aoyama, R.; et al. Measurements of Dielectron Production in Au+Au Collisions at $\sqrt{s_{\rm NN}}$= 27, 39, and 62.4 GeV from the STAR Experiment. *arXiv* **2018**, arXiv:nucl-ex/1810.10159.
75. NA60 Collaboration; Arnaldi, R.; Banicz, K.; Borer, K.; Castor, J.; Chaur, B.; Chen, W.; Cicalò, C.; Colla, A.; Cortese, P.; et al. NA60 results on thermal dimuons. *Eur. Phys. J. C* **2009**, *61*, 711–720. [CrossRef]
76. HotQCD Collaboration; Bazavov, A.; Bhattacharya, T.; Buchoff, M.; Cheng, M.; Christ, N.; Ding, H.; Gupta, R.; Hegde, P.; Jung, C.; et al. The chiral transition and $U(1)_A$ symmetry restoration from lattice QCD using Domain Wall Fermions. *Phys. Rev. D* **2012**, *86*, 094503. [CrossRef]
77. van Hees, H.; Rapp, R. Dilepton Radiation at the CERN Super Proton Synchrotron. *Nucl. Phys. A* **2008**, *806*, 339–387. [CrossRef]
78. Agakishiev, G.; Balanda, A.; Belver, D.; Belyaev, A.; Blanco, A.; Böhmer, M.; Boyard, J.L.; Cabanelas, P.; Castro, E.; Chernenko, S.; et al. Dielectron production in Ar+KCl collisions at 1.76A GeV. *Phys. Rev. C* **2011**, *84*, 014902. [CrossRef]
79. Ahdida, C.; Alocco, G.; Antinori, F.; Arba, M.; Aresti, M.; Arnaldi, R.; Roldan, A.B.; Beole, S.; Beraudo, A.; Bernhard, J.; et al. Letter of Intent: The NA60+ experiment. *arXiv* **2022**, arXiv:2212.14452.
80. Abgaryan, V.; Acevedo Kado, R.; Afanasyev, S.V.; Agakishiev, G.N.; Alpatov, E.; Altsybeev, G.; Alvarado Hernández, M.; Andreeva, S.V.; Andreeva, T.V.; Andronov, E.V.; et al. Status and initial physics performance studies of the MPD experiment at NICA. *Eur. Phys. J. A* **2022**, *58*, 140. [CrossRef]
81. Ablyazimov, T.; Abuhoza, A.; Adak, R.P.; Adamczyk, M.; Agarwal, K.; Aggarwal, M.M.; Ahammed, Z.; Ahmad, F.; Ahmad, N.; Ahmad, S.; et al. Challenges in QCD matter physics –The scientific programme of the Compressed Baryonic Matter experiment at FAIR. *Eur. Phys. J. A* **2017**, *53*, 60. [CrossRef]
82. Anderson, C.D. The Apparent Existence of Easily Deflectable Positives. *Science* **1932**, *76*, 238–239. [CrossRef]
83. Chao, C.Y. Scattering of Hard γ-Rays. *Phys. Rev.* **1930**, *36*, 1519–1522. [CrossRef]
84. Klemperer, O. On the annihilation radiation of the positron. *Math. Proc. Camb. Philos. Soc.* **1934**, *30*, 347–354. [CrossRef]
85. Breit, G.; Wheeler, J.A. Collision of two light quanta. *Phys. Rev.* **1934**, *46*, 1087–1091. [CrossRef]
86. Fermi, E. On the Theory of the impact between atoms and electrically charged particles. *Z. Phys.* **1924**, *29*, 315–327. [CrossRef]
87. Bauer, R.; Breskin, A.; Chechik, R.; Drees, A.; Faschingbauer, U.; Fischer, P.; Fraenkel, Z.; Fuchs, C.; Gatti, E.; Gläß, J.; et al. Measurement of electromagnetically produced e^+e^- pairs in distant S-Pt collisions. *Phys. Lett. B* **1994**, *332*, 471–476. [CrossRef]
88. Acciarri, M.; Adriani, O.; Aguilar-Benitez, M.; Ahlen, S.; Alcaraz, J.; Alemanni, G.; Allaby, J.; Aloisio, A.; Alverson, G.; Alviggi, M.G.; et al. Production of e, μ and τ pairs in untagged two photon collisions at LEP. *Phys. Lett. B* **1997**, *407*, 341–350. [CrossRef]
89. Adeva, B.; Anderhub, H.; Ansari, S.; Becker, U.; Becker-Szendy, R.; Berdugo, J.; Boehm, A.; Bourquin, M.; Branson, J.G.; Burger, J.D.; et al. Electroweak studies in e^+e^- collisions: $12 < \sqrt{s} < 46.78$ GeV. *Phys. Rev. D* **1988**, *38*, 2665–2678. [CrossRef]
90. The OPAL Collaboration; Abbiendi, G. Total hadronic cross-section of photon-photon interactions at LEP. *Eur. Phys. J. C* **2000**, *14*, 199–212. [CrossRef]
91. The CMS collaboration.; Chatrchyan, S. Search for exclusive or semi-exclusive $\gamma\gamma$ production and observation of exclusive and semi-exclusive e^+e^- production in pp collisions at $\sqrt{s} = 7$ TeV. *J. High Energ. Phys.* **2012**, *2012*, 80.
92. The CMS Collaboration; TOTEM Collaboration; Sirunyan, A.M.; Tumasyan, A.; Adam, W.; Ambrogi, F.; Asilar, E.; Bergauer, T.; Brstetter, J.; Brondolin, E.; et al. Observation of proton-tagged, central (semi)exclusive production of high-mass lepton pairs in pp collisions at 13 TeV with the CMS-TOTEM precision proton spectrometer. *J. High Energ. Phys.* **2018**, *2018*, 153.
93. Abdallah, M.S.; Aboona, B.E.; Adam, J.; Adamczyk, L.; Adams, J.R.; Adkins, J.K.; Agakishiev, G.; Aggarwal, I.; Aggarwal, M.M.; Ahammed, Z.; et al. Measurement of e^+e^- Momentum and Angular Distributions from Linearly Polarized Photon Collisions. *Phys. Rev. Lett.* **2021**, *127*, 052302. [CrossRef]
94. Klein, S.R.; Nystrand, J.; Seger, J.; Gorbunov, Y.; Butterworth, J. STARlight: A Monte Carlo simulation program for ultra-peripheral collisions of relativistic ions. *Comput. Phys. Commun.* **2017**, *212*, 258–268. [CrossRef]
95. Adam, J.; Adamczyk, L.; Adams, J.R.; Adkins, J.K.; Agakishiev, G.; Aggarwal, M.M.; Ahammed, Z.; Alekseev, I.; Anderson, D.M.; Aoyama, R.; et al. Observation of excess J/ψ yield at very low transverse momenta in Au+Au collisions at $\sqrt{s_{\rm NN}} = 200$ GeV and U+U collisions at $\sqrt{s_{\rm NN}} = 193$ GeV. *Phys. Rev. Lett.* **2019**, *123*, 132302. [CrossRef] [PubMed]
96. Zha, W.; Klein, S.R.; Ma, R.; Ruan, L.; Todoroki, T.; Tang, Z.; Xu, Z.; Yang, C.; Yang, Q.; Yang, S. Coherent J/ψ photoproduction in hadronic heavy-ion collisions. *Phys. Rev. C* **2018**, *97*, 044910. [CrossRef]
97. Zha, W.; Ruan, L.; Tang, Z.; Xu, Z.; Yang, S. Coherent photo-produced J/ψ and dielectron yields in isobaric collisions. *Phys. Lett. B* **2019**, *789*, 238–242. [CrossRef]
98. Wang, P.; Wu, X.; Zha, W.; Tang, Z. Calculations of differential momentum transfer spectra for J/ψ photoproduction in heavy-ion collisions. *Chin. Phys. C* **2022**, *46*, 074103. [CrossRef]
99. Kłusek-Gawenda, M.; Szczurek, A. Photoproduction of J/ψ mesons in peripheral and semicentral heavy ion collisions. *Phys. Rev. C* **2016**, *93*, 044912. [CrossRef]

100. Zha, W.; Ruan, L.; Tang, Z.; Xu, Z.; Yang, S. Coherent lepton pair production in hadronic heavy ion collisions. *Phys. Lett. B* **2018**, *781*, 182–186. [CrossRef]
101. Li, C.; Zhou, J.; Zhou, Y.J. Probing the linear polarization of photons in ultraperipheral heavy ion collisions. *Phys. Lett. B* **2019**, *795*, 576–580. [CrossRef]
102. Li, C.; Zhou, J.; Zhou, Y.J. Impact parameter dependence of the azimuthal asymmetry in lepton pair production in heavy ion collisions. *Phys. Rev. D* **2020**, *101*, 034015. [CrossRef]
103. Heisenberg, W.; Euler, H. Consequences of Dirac's theory of positrons. *Z. Phys.* **1936**, *98*, 714–732. . [CrossRef]
104. Harland-Lang, L.A.; Khoze, V.A.; Ryskin, M.G. Exclusive LHC physics with heavy ions: SuperChic 3. *Eur. Phys. J. C* **2019**, *79*, 39. [CrossRef] [PubMed]
105. ALICE Collaboration. Letter of intent for ALICE 3: A next-generation heavy-ion experiment at the LHC. *arXiv* **2022**, arXiv:2211.02491.
106. SN0755: The STAR Beam Use Request for Run-21, Run-22 and Data Taking in 2023-25 | The STAR Experiment. 2021. Available online: https://drupal.star.bnl.gov/STAR/starnotes/public/sn0755 (accessed on 1 September 2020).
107. Prospects for Measurements of Photon-Induced Processes in Ultra-Peripheral Collisions of Heavy Ions with the ATLAS Detector in the LHC Runs 3 and 4-CERN Document Server. 2018. Available online: http://cds.cern.ch/record/2641655/files/ (accessed on 4 October 2018).
108. ATLAS Collaboration. Measurement of muon pairs produced via $\gamma\gamma$ scattering in non-ultraperipheral Pb+Pb collisions at $\sqrt{s_{\mathrm{NN}}} = 5.02$ TeV with the ATLAS detector. *arXiv* **2022**, arXiv:2206.12594. [CrossRef]